

# Millennial and orbital-scale variability in a 54,000-year record of total air content from the South Pole ice core.

Jenna A. Epifanio<sup>1</sup>, Edward J. Brook<sup>1</sup>, Christo Buizert<sup>1</sup>, Erin C. Pettit<sup>1</sup>, Jon S. Edwards<sup>1</sup>, John M. Fegyveresi<sup>2</sup>, Todd A. Sowers<sup>3</sup>, Jeffrey P. Severinghaus<sup>4</sup>, Emma C. Kahle<sup>5</sup>

- 5 <sup>1</sup>College of Earth, Ocean, and Atmospheric Science, Oregon State University, Corvallis, 97331, USA  
<sup>2</sup>School of Earth and Sustainability, Northern Arizona University, Flagstaff, 86011, USA  
<sup>3</sup>The Earth and Environmental Systems Institute, Pennsylvania State University, University Park, PA, USA  
<sup>4</sup>Scripps Institution of Oceanography, University of California San Diego, La Jolla, CA, USA  
<sup>5</sup>Department of Earth and Space Sciences, University of Washington, Seattle, WA, USA
- 10 *Correspondence to:* Jenna A. Epifanio (jenna.epifanio@gmail.com)

**Abstract.** The total air content (TAC) of polar ice cores has long been considered a potential proxy for past ice sheet elevation. Recent work, however, has shown that a variety of other factors also influence this parameter. In this paper we present a high-resolution TAC record from the South Pole (SPC14) ice core covering the last 54,000 years and discuss the implications of the data for interpreting TAC from ice cores. The SPC14 TAC record shows multiple features of interest, including (1) long-term orbital-scale variability, (2) millennial-scale variability in the Holocene and last glacial period, and (3) a period of stability from 35 ka to 25 ka. The longer, orbital-scale variations in TAC are highly correlated with integrated summer insolation (ISI), corroborating the potential of TAC to provide an independent dating tool via orbital tuning. Large millennial-scale variability in TAC during the last glacial period is positively correlated with accumulation rate reconstructions as well as the  $\delta^{15}N-N_2$ , a firm thickness proxy. These TAC variations are too large to be controlled by direct effects of temperature and too rapid to be tied to elevation changes. We propose that grain size metamorphism near the firm explains these changes. We note, however, that at sites with different climate histories than the South Pole TAC variations may be dominated by other processes. Our observations of millennial-scale variations in TAC show a different relationship with accumulation rate than observed at sites in Greenland.

15  
20

## 25 1 Introduction

Total air content (TAC), the total quantity of air trapped in polar ice, has long been explored as a proxy for many past climate and paleo-environmental conditions. Air pressure, temperature, and pore volume at bubble close-off control TAC in polar ice cores, as described by the ideal gas law (Martinerie et al., 1992). Variations in

TAC can reflect changes in any of these parameters. Early work in polar ice cores focused on using TAC to  
30 reconstruct ice sheet elevation changes given the dependence of atmospheric pressure on altitude (Raynaud and  
Lorius, 1973, Raynaud and Lebel, 1979). If elevation could be cleanly extracted from TAC records this would  
provide an invaluable constraint on ice sheet models, informing our understanding of ice sheet dynamics and sea  
level change. However, while atmospheric pressure must influence TAC, the amount of air trapped in polar ice is  
also controlled by the pore volume at close-off, which has a complex relationship with local meteorological  
35 conditions as well as firn densification, making TAC a particularly complicated proxy (Eicher et al., 2016,  
Gregory et al., 2014).

The pore volume at close-off is primarily controlled by firn densification processes and is not easily  
predicted. Previous studies have shown that variations in pore volume at bubble close-off appear to dwarf the  
influence of atmospheric surface pressure variations (Schwander et al., 1989, Eicher et al., 2016, Martiniere et al.,  
40 1994, Raynaud and Lebel, 1979, Krinner et al., 2000). For temperature, Raynaud and Lebel (1979), first introduced  
a spatial correlation between site temperature and pore volume at close-off. This was later refined by Martiniere  
et al. (1992) using data from late Holocene ice core samples. This effect of temperature on pore volume can be  
empirically predicted and counteracts the effect of the local temperature from the ideal gas law. The two  
temperature effects on TAC have been shown to nearly cancel each other (Raynaud et al., 2007).

45 Previous research also showed that TAC is significantly impacted by local solar insolation on orbital  
time scales (Raynaud et al., 2007, Eicher et al., 2016). The proposed mechanism for this relationship requires that  
higher local summer insolation increases the size of snow grains in the first few meters of firn, which then  
decreases the pore volume in these same layers as they reach bubble close-off (Raynaud et al., 2007, Arnaud,  
2000). Studies at low accumulation rate polar sites have confirmed that larger firn grain sizes decrease the porosity  
50 at bubble close-off (Gregory et al., 2014, Courville et al., 2007). The relationship between TAC and local solar  
insolation on orbital time scales raises the possibility of directly dating TAC records using orbital tuning (Raynaud  
et al., 1997, Bazin et al., 2013).

On shorter, millennial timescales, in Greenland ice core records, Eicher et al. (2016) proposed that  
changes in overburden pressure of the overlying firn column, driven by changes in accumulation rate, drive an  
55 inverse relationship between pore volume at close-off and accumulation rate. This process is thought to increase  
in importance with increasing temperature, rivalling the direct impact of changes in temperature. Eicher et al.  
(2016) suggest that the accumulation rate effect on TAC may be responsible for the small millennial-scale TAC  
variations observed in Greenland ice cores. The observation is at odds with research in the low-accumulation rate  
Megadunes region of Antarctica, which seems to indicate that accumulation rate and pore volume at close-off are

60 positively correlated due to larger grain sizes in the firm at ultra-low accumulation rate sites (Gregory et al., 2014, Courville et al., 2007). However, the near-zero accumulation rate at Megadunes allows for extraordinary firm metamorphism (over hundreds of years) with the consequent reduction of pore volume, which is not comparable to Greenland.

Because previous work shows that TAC varies on multiple time scales, high-resolution data are important  
65 for fully interpreting the TAC records. To this end, we made high-resolution measurements of TAC in the South Pole ice core (SPC14). These measurements were made using a wet-extraction technique coupled with a vacuum line system that is coupled to a gas chromatograph that also provides the atmospheric methane (CH<sub>4</sub>) concentration in the same ice core sample (Epifanio, et al., 2020).

The SPC14 ice core was drilled in 2014/15 over two field seasons and reached a depth of 1751 m. The  
70 SPC14 record spans the last 54,300 years (Winski et al., 2019, Epifanio et al., 2020). The data set provides a valuable context for better constraining the complex controls on TAC in ice cores. The record shows long-term and short-term variations (Figure 1) which would not be resolved without our high-resolution measurements. In the discussion below, we compare the TAC record to solar insolation curves, as well as a variety of known climate proxies. We present a simple linear regression that explains variability in our record as a function of insolation  
75 and several other proxies. Our study supports the insolation control on TAC but also shows that other firm densification-related processes create significant millennial-scale variability, underscoring the need for high-resolution data to use TAC records for constraints on gas trapping, ice core chronologies, and even past ice-sheet elevation changes.

## 80 **2 Materials and Methods**

### **2.1 Total air content measurements**

The total air content (TAC) record from the SPC14 ice core was measured jointly in the Oregon State University (OSU) and Pennsylvania State University (PSU) ice core labs concurrently with measurements of CH<sub>4</sub>. The core was discretely sampled at approximately 1- to 2-meter resolution along the length of the core. Methods  
85 followed previous work (Epifanio, et al., 2020, Mitchell et al., 2011, Lee et al., 2020, Buizert et al., 2021) with some calibration updates described below. At OSU, the samples were measured in accordance with previously published methods (Mitchell et al., 2015, Buizert et al., 2021). The PSU samples were also measured concurrently with CH<sub>4</sub>, using a wet extraction system. The differences in methods between OSU and PSU wet extraction systems are described in Mischler et al., 2009, Fegyveresi, 2015, Epifanio et al., 2020, and WAIS Divide project

90 members, 2013. Updates to the methods at OSU allow a simple correction to the TAC measurements for variations in flask and array temperatures and volumes. The methods allowing this are described in detail below.

The OSU vacuum line is set up as portrayed in Fig. 2. Samples are melted under vacuum in a two-sided array of twelve glass vacuum flasks. The air released during the melt step is trapped in the headspace of the flasks. The melted samples are then refrozen in a -70 °C ethanol bath. Once samples are refrozen, the air trapped in the  
95 flask headspace is expanded through the array volume, isolation volume and into the gas chromatograph (GC) sample loop. In the equations below, the quantity of air in the entire vacuum line (in moles) at this point is designated  $n_1$ . The relevant array valve is then closed, trapping air upstream of the isolation and GC volumes (Figure 2). This quantity of air is designated  $n_2$ . The pressure in the GC volume is recorded by a capacitance manometer (rated at 0-100 torr, 1.5 % accuracy, P<sub>1</sub>) The air in the GC sample loop is then injected into the GC  
100 column and measured for CH<sub>4</sub> concentration using a 6890N Agilent gas chromatograph with flame ionization detector. Once the analysis is complete, the gas remaining in the GC and isolation volumes (Figure 2) is evacuated. The remaining air from the relevant array is then expanded into the GC section, the relevant array valve is then again closed, trapping air upstream of the isolation and GC volumes (Figure 2). In total, we make four expansions and four measurements of CH<sub>4</sub> concentration, and four measurements of GC pressure per sample. We assume that  
105 the temperatures of the vacuum line and GC do not change during the repeated expansions. TAC is derived from the sample mass and pressure measurements during the analysis, following the ideal gas law:

$$n = \frac{PV}{RT_{eff}}, \quad (1)$$

110 Where  $P$  is Pressure,  $V$  is volume,  $n$  is moles of air,  $T_{eff}$  is effective temperature (K) or weighted mean temperature of the various sections of the vacuum line, and  $R$  is the universal gas constant, 8.314 Jmol<sup>-1</sup>K<sup>-1</sup>.

The effective temperature of the line can change from day to day due to differences in air temperature, ethanol bath temperature, chiller efficiency, and flask headspace variation due to sample size. Because of the daily variation, it is problematic to use a weighted average calculation of  $T_{eff}$  in our calculation of TAC, as this would  
115 require a daily estimate of  $T_{eff}$  or an assumption that it is constant. To avoid this issue, we take advantage of the methods for CH<sub>4</sub> measurement. During the CH<sub>4</sub> measurement, we expand the air released from the melted ice in four expansions, with each subsequent expansion releasing lower pressures from the flask headspace. The ratio between the subsequent expansion pressures allows us to calibrate the TAC measurement, as follows.

Because the amount of air in the first expansion is equal to the amount in the second expansion plus what  
 120 was removed by evacuation:

$$n_1 = n_2 + n_{rem} \quad (2)$$

Where  $n_1$  is the amount of air in the line during the first expansion,  $n_2$  is the amount of air in the line during the  
 125 second expansion, and  $n_{rem}$  is the amount of air removed in the first expansion, and:

$$n_1 = \frac{P_1 V_T}{RT_{eff}}, \quad n_2 = \frac{P_2 V_T}{RT_{eff}}, \quad n_{rem} = \frac{P_1 V_{gc}}{RT_{gc}} \quad , \quad (3)$$

where  $P_1$  is the pressure of the first expansion,  $V_T$  is the total volume of the vacuum line and GC, and  $V_{gc}$  and  $T_{gc}$   
 130 are the volume and temperature of the vacuum line past the GC valve. Following from equation (2),

$$\frac{P_1 V_T}{RT_{eff}} - \frac{P_2 V_T}{RT_{eff}} = \frac{P_1 V_{gc}}{RT_{gc}} \quad (4)$$

Rearranging to solve for  $\frac{T_{gc}}{V_{gc}}$  :

135

$$\frac{T_{gc}}{V_{gc}} = \frac{T_{eff} P_1}{V_T (P_1 - P_2)} \quad (5)$$

and then rearranging to solve for  $T_{eff}$

$$140 \quad T_{eff} = V_T \frac{P_1 - P_2}{P_1} \frac{T_{gc}}{V_{gc}} \quad (6)$$

TAC is calculated by dividing  $n_1$  by sample mass. To eliminate the need to measure  $T_{eff}$  every time TAC is  
 calculated, we use  $T_{eff}$  from equation 6 in the calculation of TAC:

$$145 \quad \frac{n_1}{m} = \frac{P_1^2}{R(P_1 - P_2)} \frac{T_{gc}}{m V_{gc}} \quad (7)$$

We then substitute R in equation (7) for the ideal gas law, with a final calculation for TAC:

$$TAC = \frac{P_1^2}{R(P_1 - P_2)} \frac{T_{gc} T_{STP}}{m V_{gc} P_{STP}} \quad (8)$$

150

For comparison with previous work we convert to units of cm<sup>3</sup> STP g<sup>-1</sup>. Equation (8) requires that we have an accurate measure of  $\frac{T_{gc}}{V_{gc}}$ . Two separate methods were used to achieve this. The first method involved estimating  $T_{eff}$  by taking a weighted average of the system temperature with the GC oven at 50 °C and the flasks submerged in a -70 °C ethanol bath. Once a known amount of air was expanded into the GC,  $\frac{T_{gc}}{V_{gc}}$  was calculated.

155 The line temperature for the portion outside the GC oven was estimated by averaging the measured temperature at multiple points adjacent to the line. The variation in temperature of the line was less than 0.1 °C. The final value of  $\frac{T_{gc}}{V_{gc}}$  determined using this method was 12.37 (Kcc<sup>-1</sup>).

The second calibration did not use the chilled flasks and instead utilized a removable known volume of air that was externally attached to the vacuum line. From expansions of air to other parts of the array and GC, we were able to calculate the volume of the entire system and individual components and the GC. All volumes are listed in Table 1. Air was expanded into the entire system at a known pressure, with the GC at room temperature (21.5 °C). The front array valve was closed, isolating the pressure in the front array, while the rest of the line was pumped to vacuum. After the pressure stabilized, the air in the front array was expanded to the entire line, and the pressure was recorded. Finally, the GC oven was switched on and raised to the normal operating temperature (50 °C). The pressure in the total line after heating was recorded as  $P_{eff}$ . To solve for  $T_{eff}$ , we use the combined gas law:

$$\frac{P_1 V_1}{T_1} = \frac{P_2 V_2}{T_2} \quad (9)$$

170 Where  $P_1 = P_{array}$  is the pressure of the air in the front array with the line at room temperature,  $V_1 = V_{array}$  is the volume of the front array,  $T_1$  is the measured lab temperature,  $P_2 = P_{eff}$  or the pressure of the air in the entire system, including both array volumes, isolation volume, and the GC volume, and  $T_2 = T_{eff}$  or the effective temperature of the entire system with the GC at 50 °C. Rearranging equation (9) to solve for  $T_2$  (or  $T_{eff}$ ):

$$175 \quad T_{eff} = \frac{P_{eff}V_T T_{array}}{P_{array}V_{array}} \quad (10)$$

Finally, multiple expansions of air from the front array to the GC volume consistently give a ratio of pressures (between the four subsequent expansions for one measurement) of 0.56. Combined with equation (5), this ratio yields a final  $\frac{T_{gc}}{V_{gc}}$  of 12.79 (K/cc). This value is different from the original value of 12.37 (Kcc<sup>-1</sup>) but we  
 180 believe is more accurate due to the difficulty of estimating  $T_{eff}$  during the first calibration. The second method also removes the variability of flask size and accounts for small changes made in the vacuum line over time. All measurements of TAC on the SPC14 ice core were calibrated using the  $\frac{T_{gc}}{V_{gc}}$  value of 12.79 (Kcc<sup>-1</sup>).

## 2.2 Solubility and cut bubble corrections

185 Two small corrections were made to the TAC measurements to account for effects on TAC introduced during sample preparation and measurement. Because the air trapped in the headspace of the flask is not allowed sufficient time to reach solubility equilibrium during the melt refreeze process, a correction was made to account for the residual gas trapped in the refrozen ice. Following Mitchell et al. (2015), we determined an empirical TAC solubility correction of +1.3 %, which we added to all sample measurements. This empirical correction was  
 190 derived during wet extraction by measuring the TAC remaining within the flask headspace after a second melt-refreeze cycle.

The second correction accounts for the air lost during cutting and trimming the ice samples. Preparing ice-core samples for measurement unavoidably cuts through some bubbles, releasing a fraction of the air content from the entire ice sample. As a result, measurements made of the total air are slightly lower than true values.

195 This cut-bubble correction is based on a statistical relationship between the total number and average size of bubbles in a given sample, and the amount of exposed surface area that is cut during sample preparation (Saltykov, 1976). Bubble numbers and average sizes were determined during number-density, physical property measurements, and micro-CT measurements as described in Fegyveresi et al. (2011), Fitzpatrick et al. (2014), and Fegyveresi et al. (2018). Following the methods in Matinerie et al. (1990) and Fegyveresi (2015), we interpolated  
 200 the bubble size and density to each TAC sample, and applied the correction based on the bubble size distribution for each sample across the dataset. To estimate the exposed surface area of each sample, we used standard rectangular dimension (2.5 cm x 2.5 cm x 9 cm), and a mass of 51.2 g across all samples. There is likely some missed variation due to trimming on the edges of samples, but the variation is small. The cut-bubble correction

indicates a maximum of 8 % loss in the first 200 m of ice, decreasing to 1.9 % TAC loss at the base of the bubbly  
205 ice at ~1200m, at the onset of the clathrate-ice transition. The correction is shown in Fig. 3. While clathrate ice  
will still have a gas-loss correction, it is likely constant and no more than 1.9 %. We applied no correction below  
the base of the bubbly ice.

### 3 Results and Discussion

#### 3.1 South Pole total air content record

210 The SPC14 ice core TAC record is shown in Fig. 1, plotted on the SPC19 ice age scale (Winski et al., 2019). We  
plot our data on the ice-age scale, rather than the gas-age scale, given evidence that ice-sheet surface conditions  
have a major impact on the pore volume at bubble close-off (further discussed below). This convention is  
consistent with previous research (Eicher et al, 2016, Raynaud et al, 2007). Using the method described above,  
we measured TAC concurrently with the SPC14 CH<sub>4</sub> record (Epifanio et al., 2020), resulting in a total of 2,318  
215 measurements made on samples at 1,067 individual depths. Samples were taken at approximately every meter  
along the depth range from 131 to 1,751 m, which spans the period of 130 to 54,302 years BP. The age resolution  
of these samples is the same as reported for CH<sub>4</sub> in the SPC14 ice core, averaging 42 years, but increasing from  
20 years in the Holocene to 190 years at the bottom of the ice core record (Epifanio et al., 2020).

The OSU data set has a pooled standard deviation of 0.0006 cm<sup>3</sup>g<sup>-1</sup> and the PSU data set (130 -1150 m)  
220 has a pooled standard deviation of 0.002 cm<sup>3</sup>g<sup>-1</sup>. Differences in methods between the OSU and PSU labs created  
a mean offset of 0.0072 cm<sup>3</sup>g<sup>-1</sup>. To correct for this offset, PSU values were increased to be comparable to OSU  
values. The pooled standard deviation of measurements for the combined dataset (130 – 1150 m) is 0.002 cm<sup>3</sup>g<sup>-1</sup>,  
and data from 1151 -1751 m have a pooled standard deviation of 0.001 cm<sup>3</sup>g<sup>-1</sup>. Data are available at the USAP  
data repository (<https://doi.org/10.15784/601546>) including details of uncertainties and sample resolution of  
225 datasets (Epifanio, et al., 2022). To our knowledge this is the first ice core TAC record with this resolution and  
length, allowing in-depth comparison with other climate proxies at a site that is not likely to have experienced  
significant elevation change over the last 54 ka (Fudge et al., 2020, Lilien et al., 2018).

The SPC14 TAC record has several notable characteristics (Figure 1). Long term trends include an  
increase in TAC from 53 ka to 36 ka, followed by an approximately 10 ka period of low variability, then decreasing  
230 TAC from about 20 ka to the present. Millennial-scale variations, both in the Holocene and glacial period, consist  
of large magnitude abrupt changes. These variations are as large as 0.007 cm<sup>3</sup>g<sup>-1</sup> in 2,600 years, which is 47 % of  
the total amplitude in the record. Higher frequency variations exist on centennial or shorter timescales that may



represent firm processes such as layering, but our sampling resolution is not adequate to fully evaluate this possibility.

### 235 3.2 Impacts of temperature on TAC

Prior work suggests that temperature impacts TAC in two ways, the first through the ideal gas law, and the second through an empirically established relationship between the pore volume at bubble close-off and temperature (Martinerie et al., 1992). Given a fixed pore volume at close-off, TAC is given by the ideal gas law:

$$240 \quad TAC = V_c * \frac{P_c}{T_c} * \frac{T_0}{P_0} \quad (11)$$

Where TAC is the total air content ( $\text{cm}^3\text{g}^{-1}$ ),  $V_c$  is the pore volume at close off ( $\text{cm}^3\text{g}^{-1}$ ),  $P_c$  and  $T_c$  are pressure and temperature of the air contained in  $V_c$  at close-off (mb and K), and  $P_0$  and  $T_0$  are standard pressure and temperature (1013 mb and 273 K, respectively).

245 The empirical relationship between pore volume and temperature, as found by Martinerie et al. (1992) is given by:

$$V_c = (7.6 * 10^{-4}) * T_s - 0.057 \quad (12)$$

250 Where  $T_s$  is the surface temperature (K).

To examine direct thermal effects, we follow Raynaud et al. (2007) and Eicher et al. (2016) to define a non-thermal residual term  $V_{cr}$ :

$$V_{cr} = TAC * \frac{T_c}{P_c} * \frac{P_0}{T_0} - V_c \quad (13)$$

255 We use the same temperature for the surface ( $T_s$ ) and the close-off depth ( $T_c$ ). While the temperature at pore close-off ( $T_c$ ) is a bit warmer than  $T_s$  due to geothermal heating, the difference is small when the firm column is in equilibrium. For the temperature at bubble close-off ( $T_c$ ), we used a temperature reconstruction from Kahle et al. (2021). To approximate  $P_c$ , we use value of 680 mb at the surface of the ice core, linearly decreasing with depth to account for 180 m of elevation increase upstream of the drill site (NOAA GML, 2020, Fudge et al., 2020).

260 Following Raynaud et al. (2007) and Lipenkov et al. (2011), we then create standardized versions of TAC and  $V_{cr}$ , called TAC\* and  $V_{cr}$ \*, in order to compare TAC and the non-thermal residual. The standardized

data sets were created by subtracting the mean value (of TAC or  $V_{cr}$ , respectively) and then dividing by the respective standard deviation. These data are plotted together in Fig. 4. The correlation between TAC\* and  $V_{cr}$ \* is very high ( $r^2 = 0.96$ ).  $V_{cr}$ \* is a quantity that describes TAC if temperature did not affect pore volume at close-off, and is useful for understanding the magnitude of the direct effects of temperature. The very high correlation between TAC\* and  $V_{cr}$ \* agrees with previous work on both EDC and NGRIP ice cores that show the direct temperature effect on TAC is responsible for a very small amount of TAC variability. As a result, we targeted our analysis using measured TAC instead of the non-thermal residual.

### 3.3 Orbital-scale variations in TAC

Local integrated summer insolation (ISI) has shown an anti-correlation with TAC in various Antarctic and Greenland ice cores (Raynaud et al., 2007, Lipenkov et al., 2011, Eicher et al., 2016). South Pole is an interesting site to study in this regard, as it is the only place in Antarctica without a diurnal cycle in solar insolation. Following Huybers et al. (2006) and Raynaud et al. (2007) we find ISI by:

$$ISI = \sum \beta_i (\omega_i * 86,400) \quad (14)$$

where ISI is in joules,  $\omega_i$  is the daily insolation in  $Wm^{-2}$ , and  $\beta_i$  is a Heaviside step function, where  $\beta_i = 1$  when  $\omega_i$  is  $> \omega_{threshold}$ , otherwise  $\beta_i = 0$ . ISI is impacted by a mix of precession and obliquity and the curves are unique for latitude and the chosen  $\omega_{threshold}$ .

Earlier research emphasized the anti-correlation between ISI and TAC and used the relationship to orbitally tune the ages of Antarctic ice core records (Lipenkov et al., 2011, Raynaud et al., 2007, Parrenin et al., 2007). Conclusions of previous work suggest that the insolation effect is much larger than the direct effects of temperature discussed above and is found in both Northern and Southern Hemisphere records (Eicher et al., 2016).

We find a maximum anti-correlation of ISI with TAC at a cutoff threshold of  $225 Wm^{-2}$  ( $r^2 = 0.46$ ,  $p < 0.0001$ ). Studies of the same relationship in the EDC and NGRIP ice cores found maximum correlations at different cutoff values ( $390 Wm^{-2}$  for NGRIP with  $r^2 = 0.3$ ) (Eicher et al., 2016, Raynaud et al., 2007). However, the correlation difference between varying threshold values (0 to  $500 Wm^{-2}$ ) is small ( $r^2 = 0.42$  to  $r^2 = 0.46$ ). The linear regression of TAC as a function of ISI at a threshold cutoff of  $225 Wm^{-2}$  is shown in Fig. 5. To make this calculation, we interpolated the ISI data to the ages assigned to TAC.

The ISI regression misfit values show an even distribution. The link between TAC and ISI supports the proposition that TAC can be used for absolute (orbitally tuned) dating of ice cores (Raynaud et al., 2007). It is

worth noting, however, that the SPC14 TAC record only covers the last 54,000 years, which is only slightly longer than one obliquity cycle. This time period is shorter than the ice core records mentioned above, which may affect the differences in cutoff threshold that give maximum correlation between TAC and ISI.

### 295 3.4 Millennial-scale variations observed in TAC

While the ISI appears to be highly correlated with long-term variations in TAC, it fails to explain the observed millennial-scale changes. Abrupt, large magnitude, millennial-scale variations in TAC exist through the Holocene and early part of the glacial period. The approximate magnitude of the largest, abrupt millennial-scale changes is  $0.007 \text{ cm}^3\text{g}^{-1}$  in  $\sim 3$  kyr, which is similar to the abrupt millennial-scale variations observed in NGRIP, 300 which were typically around  $0.01 \text{ cm}^3\text{g}^{-1}$  in the same time frame (Eicher et al., 2016). Millennial-scale variations are absent from 40 ka to 22 ka in the SPC14 ice core, but high frequency (centennial-scale and smaller) variations persist through the entire record. The existence of millennial-scale and higher frequency variations underscores the need for high-resolution data to discern the long-term patterns from other climatic effects on TAC. We isolate the millennial-scale TAC variations by subtracting the orbital-scale trends that we find via regression of TAC onto 305 ISI (Figure 5). The largest millennial-scale features occur at 52 ka, 46 ka, and 44 ka. Similar large features are not found between 43 ka and 25 ka, where the TAC reaches a maximum, steady value of about  $0.11 \text{ cm}^3\text{g}^{-1}$ . Large variations resume at 22 ka and occur through the Holocene time period, mostly between 9 ka and 2 ka.

We first investigate the possibility of surface pressure changes driving the millennial-scale variability. Using the relationship of air pressure with TAC (Eq. 11) as proposed by Martinerie et al. (1992), we calculated 310 the pressure change required for a representative high-frequency TAC change. For example, the abrupt increase in TAC of  $0.01 \text{ cm}^3\text{g}^{-1}$  in 2.7 kyr starting at 49.2 ka (Figure 1) would require a mean pressure change of 104 hPa over that time interval. In the absence of elevation change, central Eastern Antarctica could not likely sustain large atmospheric pressure changes for that length of time. Hourly atmospheric pressure measurements at the South Pole are between 710 and 650 hPa, varying on seasonal timescales (NOAA GML, 2020). However, daily, or even 315 seasonal, variations in pressure would not be recorded in our TAC record due to the gradual bubble trapping process that takes decades to complete. Current spatial gradients of sea level pressure, including variations associated with the Amundsen Sea Low (ASL), show a maximum range of about 50 mb from maximum low to high pressure over Antarctica (Schneider et al., 2012, Raphael et al., 2016). A change in atmospheric pressure large enough to explain these TAC variations would require a dramatic reorganization of the westerly winds, 320 which is highly unlikely during the last glacial period. Some modeling studies have examined wind changes around Antarctica, using 10,000-year model runs, and found moderate changes in sea level pressure, no greater

than 15 hPa (Goodwin et al., 2014). The wind effect, as described in Martinerie et al. (1994) would require large, sustained wind changes over millennia that are not supported by modeling reconstructions (Goodwin et al., 2014).

325 If the TAC change were entirely explained by a surface pressure change induced from ice sheet elevation changes, an elevation change of about 1,200 meters would be needed. Such a large and abrupt change is unlikely to have been driven by accumulation change alone and is otherwise not likely due to the geographical context of the South Pole. Accumulation rates during the glacial period were just 3 cm $yr^{-1}$  (water equivalent), which would mean the maximum amount of elevation gain due to accumulation alone would be only about 80 meters, without considering the effects of ice layer thinning.

330 The location of SPC14 in the interior of Eastern Antarctica means that it would not have been subject to large elevation changes associated with major climate transitions, especially during the beginning of the last glacial period (Golledge et al., 2014, Fudge et al., 2020). The SPC14 ice core was not drilled at an ice divide, which means the ice collected at the South Pole flowed over topography before it arrived at the sampling location. This flow changed the local elevation at which the snow fell in the past. The history of ice flow of the SPC14 ice core, however, is not constrained beyond 100 km from the core site and is best constrained in the closest 65 km, 335 representing the last 10 ka, or about 725 m ice core depth (Lilien et al., 2018, Fudge et al., 2020). Following the ice flow line upstream from the modern ice core site shows the bedrock elevation only varying by about 500 m, which corresponds to an ice surface elevation variation of about 300 meters during that time (Lilien et al., 2018, Fudge et al., 2020, Kahle et al., 2021, Morgan et al., 2022). This 300 m change is much less than the 1200 m 340 change required by our millennial-scale TAC observations. Large transient features in surface ice sheet elevation do not exist, eliminating ice flow as a source of abrupt elevation change influencing TAC.

Other hypotheses for changing TAC include layering due to melt, and dust affecting grain metamorphism. Layering due to melt or other effects influences the trapping of air in ice, shaping TAC but is not relevant here to the lack of melt layers. Dust has also been documented to influence grain metamorphism in the 345 firn. Due to its interior location, the ice at South Pole experiences very small changes in dust flux. We observe no correlation between dust deposition and TAC.

### 3.4.1 Accumulation

Since we can reasonably show that large millennial-scale changes in TAC are not due to direct effects of temperature, variations in air pressure or ice dynamics, pore volume at bubble close-off must account for most of 350 the TAC variations. Two observations are important to help explain these changes as a function of pore volume

at close-off: (1) a positive correlation between TAC and accumulation rate, and (2), a high positive correlation between TAC and  $\delta^{15}N-N_2$  in trapped air in the core.

First, the millennial-scale changes in TAC are highly correlated with the accumulation rate reconstruction from Kahle et al. (2021), also plotted on the SP19 ice age ( $r^2 = 0.59$ ,  $p < 0.001$ , Figure 6 and Table 2). Kahle et al. (2021) calculated the accumulation rate by using an inverse method which used models of firn densification, water isotope diffusion, and layer thinning to predict an accumulation rate history based on constraints provided by measured  $\Delta$ age, diffusion length, and annual layer thicknesses. The first 11.3 ka of the Kahle et al. (2021) reconstruction incorporates measured annual layer thicknesses from the layer counted time scale from Winski et al. (2019). This results in an accumulation record that closely resembles the previous accumulation rate history from Winski et al. for this section of the core.

Second, the millennial-scale changes in TAC are also highly correlated with  $\delta^{15}N-N_2$  when plotted on the SP19 gas age scale ( $r^2 = 0.51$ ,  $p < 0.001$ , Figure 6 and Table 2). This observation is consistent with the idea that millennial-scale fluctuations in accumulation drive similar-scale changes firn thickness, which affects  $\delta^{15}N-N_2$  due to gravitational fractionation (Severinghaus et al., 1998, Sowers et al., 1992, Morgan et al., 2022). As temperature variations are relatively minor at the South Pole, it is accumulation variation that drives the observed changes in SPC14  $\delta^{15}N-N_2$ . At this site, greater accumulation rates cause a thicker firn column and a subsequently higher  $\delta^{15}N-N_2$ . Because  $\delta^{15}N-N_2$  is not set until pore close-off, toward the base of the firn, comparison of the effect in  $\delta^{15}N-N_2$  with accumulation rate is done using the gas age scale for  $\delta^{15}N-N_2$  and ice age scale for TAC. Winski et al. (2019) also notes the close resemblance of  $\delta^{15}N-N_2$  and the Holocene accumulation rate reconstruction, which is further evidence to support the use of  $\delta^{15}N-N_2$  as an indicator of accumulation rate changes in SPC14. TAC was compared with temperature reconstructions as well as  $\delta^{18}O_{ice}$ . Low r-values were recorded, and the results are listed in Table 2. Note that Kahle et al. (2021) do not use the  $\delta^{15}N-N_2$  data in their inversion method.

Metamorphism of the ice in the first few meters of the firn may explain the link between accumulation rate and TAC. Lower accumulation rates allow grains to remain at or near the surface for a longer time, giving grains in the firn more time to grow while they remain at the surface (Courville et al., 2007). The size of the firn grains at the surface seems to predict the density at which bubble close-off occurs, with larger-grained firn closing off at a higher density (Arnaud, 1997; Gregory et al, 2014). Because ice density is, by definition, inversely proportional to porosity, higher-density bubble close-off (associated here with longer time near the surface of the ice sheet, larger grain sizes, and lower accumulation) leads to bubbles with less pore volume than firn with smaller grain sizes. Lower accumulation rates may additionally allow more time for grains to become spherically shaped before close-off, where higher accumulation rates tend to close off bubbles earlier in the densification process.

Because grains tend to move toward a spherical shape with enough time, due to vapor diffusion (Eicher et al., 2016), low accumulation rates likely create more homogeneous, spherically shaped grains. These spherically shaped grains could force more air to escape the ice core, leading to lower TAC. (Gregory et al., 2014) noted  
385 higher gas diffusivity at lower accumulation sites, implying that at low accumulation sites, the pores are closing off later, allowing time for more spherically shaped grains. We propose that a mechanism of grain size and shape affecting pore volume leads to a positive correlation between accumulation and TAC, which we observe in the SPC14 ice core, however the microstructure and physics behind the mechanism should be explored in future work.

In a sense, this proposed grain size mechanism is similar to the proposed mechanism for how ISI impacts  
390 TAC on an orbital timescale (Raynaud et al., 2007, Eicher et al., 2016). ISI is hypothesized to act on TAC by changing the grain size of the firn at the surface by influencing temperature gradients in the first few meters of firn. On orbital time-scales, higher ISI increases the near-surface firn metamorphism and grain size, and decreases pore volume at close off, resulting in the inverse relationship between TAC and ISI recorded in both hemispheres (Raynaud et al., 1997, Eicher et al., 2016). In our proposed mechanism for millennial-scale variations in TAC,  
395 lower accumulation increases near-surface firn metamorphism and grain size and decreases pore volume at close-off. In both scenarios (orbital- and millennial-scale changes), grain size is set in the first few meters of the firn, though by different mechanisms, and the impact is advected to the close-off depth. We propose that the relationship between grain size and accumulation rate is responsible for the large, millennial-scale changes in TAC found in the SPC14 ice core. This mechanism is complimentary to the orbital changes in TAC imposed by  
400 ISI and creates millennial-scale changes imposed on top of the orbital-scale changes.”

Studies of TAC in Greenland suggest a different mechanism for similar-magnitude changes in TAC. Eicher et al. (2016) observed a complex, asynchronous relationship between rapid climate changes (D-O events) and millennial-scale TAC changes in the NGRIP ice core. Figure 7 shows the Greenland (North GRIP) TAC record compared with accumulation the same site. Eicher et al. (2016) suggest the relationship is due to step  
405 changes in accumulation rate and temperature during D-O events in Greenland, causing the firn to densify rapidly due to increased load changes. This hypothesis is not consistent with our results in the SPC14 ice core, perhaps because the load changes in Antarctica are not nearly as large or abrupt as observed in Greenland. Accumulation rate changes at the South Pole during the glacial period are much smaller than in Greenland ( $1 \text{ cm yr}^{-1}$  or 25 % change over an AIM event, compared with  $10 \text{ cm yr}^{-1}$  or 100 % increase during a D-O event in Greenland), while  
410 the TAC changes at both locations are of a similar magnitude ( $0.007 \text{ cm}^3 \text{ g}^{-1}$  at SPC14,  $0.005 \text{ cm}^3 \text{ g}^{-1}$  at NGRIP). This suggests that the accumulation effect on TAC scales differently at NGRIP when compared to SPC14, implying that the two locations respond differently to accumulation changes. Interpreting TAC at any ice core

requires a universal explanation of how the firm densifies, and future work may elucidate a single mechanism that can explain the TAC-accumulation relationship at both polar regions. For example, we hypothesize that the grain  
415 size mechanism dominates at colder, dryer locations, and the mechanism requiring transient firm densification  
would prevail when warmer, wetter conditions exist. High-resolution TAC datasets across a suite of climate  
conditions are needed to test this hypothesis.

### 3.5 Multiple regression to further investigate controls on TAC

A multiple-regression analysis was performed to examine how climate-related variables correlate with  
420 TAC at SPC14. This analysis was performed to examine the possibility of removing non-elevation-dependent  
signals from the record. Because we do not expect large elevation changes at the South Pole site, SPC14 is an  
excellent ice core to examine this possibility. If the TAC variability in the SPC14 core can be explained using  
measured or modeled climate variables, it might be possible in future projects to extract the portion of the  
variability due to elevation change. Here we considered two separate multiple linear regression analyses. In the  
425 first multiple regression (referred to as the ‘modeled reconstruction’ multiple regression), we examined the  
relationship between TAC, ISI and accumulation rate. In the second multiple regression (referred to as the  
‘measured data’ multiple regression), we examined links between TAC and ISI and  $\delta^{15}\text{N}-\text{N}_2$ . TAC data and  
variables considered are plotted in Figure 8.

The modeled reconstruction regression included TAC, ISI, and the Kahle et al. (2021) reconstruction of  
430 accumulation rate. The modeled reconstruction multiple regression had a maximum adjusted  $r^2 = 0.51$  ( $p < 0.0001$ ), therefore the combined relationship accounts for 51% of the variation in the SPC14 TAC. The modeled  
reconstruction multiple regression residuals show an even distribution. The parameters are listed in Table 3 in  
order of how much each parameter affected the adjusted correlation coefficient.

The regression using only measured parameters incorporated  $\delta^{15}\text{N}-\text{N}_2$  instead of using the modeled  
435 accumulation rate. Results are listed in Table 3. We find a maximum adjusted  $r^2 = 0.62$  ( $p < 0.0001$ ). Both the  
modeled and measured parameter multiple regressions compare well (Figure 9).

For both the modeled and measured regression models, addition of other climate variables increased the  
goodness of fit. Adding temperature and  $\Delta\text{age}$  to the modeled multiple regression increased the  $r^2$  to 0.72. Adding  
 $\delta^{15}\text{N}-\text{N}_2$  and  $\delta^{18}\text{O}_{\text{ice}}$  to the measured parameter multiple regression increased the  $r^2$  to 0.69. While adding these  
440 parameters increased the goodness of fit of the models, suggesting that they do record phenomena important to  
controlling TAC, the other climate parameters are also highly correlated between themselves, which makes the  
interpretation of the regression parameters difficult (Gregorich et al., 2021).

Large misfits between the multiple regression solution and measured TAC seem to occur during times when the climate is rapidly changing. An interesting feature of this analysis is that if the derivative of  $\Delta\text{age}$  ( $d\Delta\text{age}/dt$ ) is added to the multiple regression, it seems to explain more of the variability observed in the TAC record. A comparison between a regression that includes  $d\Delta\text{age}/dt$ , and a regression that does not is shown in Figure 9. Specifically,  $d\Delta\text{age}/dt$  seems to correlate well with the magnitude of TAC change that occurs at 2,600 years as well as the large variations that occur between 45 ka and the oldest part of the record. A regression analysis that includes  $d\Delta\text{age}/dt$  and the measured parameters (ISI,  $\delta^{15}\text{N}-\text{N}_2$ ,  $\delta^{18}\text{O}_{\text{ice}}$ , and  $\Delta\text{age}$ ) gives an adjusted  $r^2$  of 0.77 ( $p < 0.0001$ ), meaning that  $d\Delta\text{age}/dt$  and its interactions describe about 8 % of the measured data multiple regression solution. Adding  $d\Delta\text{age}/dt$  to the modeled reconstruction multiple regression increases the  $r^2$  adjusted by 4 %.

A possible explanation for why  $d\Delta\text{age}/dt$  explains this extra variation is that  $\Delta\text{age}$  responds to changing climate conditions, and times when  $\Delta\text{age}$  is changing rapidly (large  $d\Delta\text{age}/dt$ ) correspond with large changes in temperature and accumulation rate not tracked adequately with other variables. We specifically observe this at D-O 12 and 13. This agreement between large  $d\Delta\text{age}/dt$  and rapid climate changes again points to a mechanism in the firn column that responds to transient accumulation changes. Following the reasoning of Eicher et al.(2016), times of large changes in accumulation may not allow the firn to form spherical bubbles, creating less pore space, and therefore lower TAC values.

An observation that is not explained by the multiple regression is the apparent lack of TAC variability between 25 ka and 42 ka. This section of the record seems to stop responding to millennial-scale forcing. In fact, our multiple regression predicts millennial-scale changes during this time that are not realized in the TAC record, most notably a large, predicted change around 32 ka that is not reflected in TAC. A possible explanation for the lack of variation could be that the effect of accumulation rate on TAC is inhibited when ISI is at a minimum. This inhibition of accumulation effects on grain size could be due to ISI dominating the grain metamorphism mechanism during that period. However, more detailed studies including high resolution TAC through multiple orbital cycles would be needed to address this question.

#### 4 Conclusion

We present a high-resolution total air content record from the SPC14 ice core covering the last 54 kyr. The implications of the analysis of the record are twofold. First, this study strongly confirms previous research on Greenland (NGRIP and GRIP) ice cores as well as Antarctic ice cores (EDC) that shows that low-frequency



variations in TAC depend on local summer insolation. Importantly, the high correlation with integrated summer insolation (ISI) corroborates the potential to orbitally tune ice age scales using TAC. Second, because the SPC14 ice core was drilled at a location with relatively small expected elevation changes over the course of the ice core history, it provides a good location to study controls on TAC outside the influence of elevation changes. Our results suggest that temperature, accumulation rate, and other firn column properties interact together to affect TAC and provide important context for developing paleoelevation proxies in cores that may have experienced large elevation changes.

We propose that a common mechanism, grain size metamorphism in the top few meters of the firn, can explain both orbital and millennial-scale times scale of TAC variations in the SPC14 ice core. Although our data are consistent with an orbital scale impact of ISI on TAC, and an accumulation-driven millennial component, further work is needed. Future directions should include:

(1) High-resolution sampling of TAC in multiple ice cores. High-resolution data are required to resolve all millennial-scale features in TAC. These features need to be accounted for before applications like paleoelevation constraints. Data should be collected for both Northern and Southern Hemisphere ice cores, and at a variety of accumulation rate regimes.

(2) Further understanding of links between  $\delta^{15}N-N_2$ ,  $\Delta_{age}$ , and TAC in ice cores. Accumulation rate can influence the  $\delta^{15}N-N_2$  and  $\Delta_{age}$  depending on climate, and therefore influence the TAC differently at different sites. High-resolution sampling of  $\delta^{15}N-N_2$  in ice cores, and model-independent  $\Delta_{age}$  determinations, could be used in future work to corroborate findings from the SPC14 ice core. Additionally, TAC sampling at locations with well-known accumulation rate histories will provide further constraints.

(3) Comparison of TAC in regions that have stable elevation histories to regions with unstable elevation histories. Ice cores targeted in coastal regions with hypothesized unstable elevation histories, such as in Western Antarctica, should be targeted for future TAC research.

### **Data Availability**

The SPC14 total air content record is published on and can be accessed through the USAP Data Center with DOI: <https://doi.org/10.15784/601546>.

### **Author Contributions**

505 JAE, EJB, JSE, TAS, JPS, JMF, ECK contributed data to this study. JAE, EJB, CB, JSE, TAS, measured ice core  
gases. ECK and JPS made isotope measurements. JMF made bubble density and size measurements. EJB and  
TAS provided funding acquisition for the study. JAE, EJB, ECP, CB, JSE, JMF, JPS, wrote, reviewed and edited  
the paper with input from all authors.

### **Competing Interests**

510

The authors declare that they have no conflict of interest.

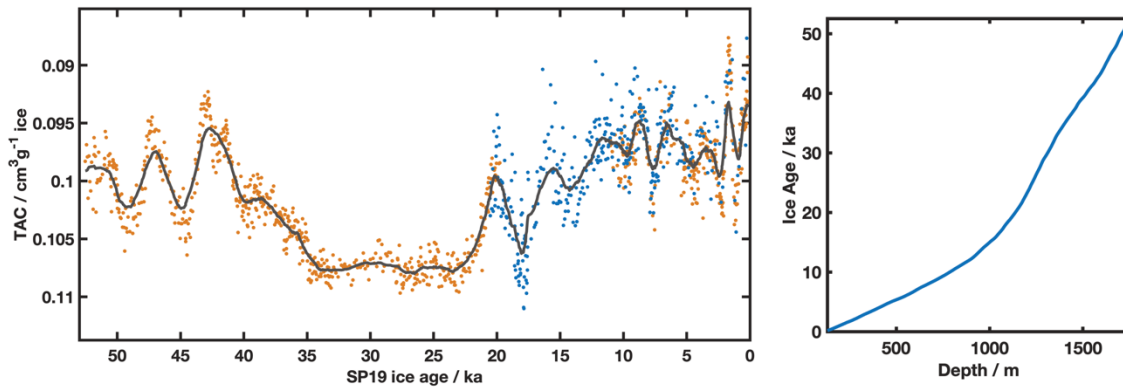
### **Acknowledgements**

515 This work has been funded by the National Science Foundation (Awards 1643722, 1443472, and 1443464). We  
would like to thank Mark Twickler and Joe Souney for their work administering the SPICEcore project; the U.S.  
Ice Drilling Program for collecting the SPC14; the field team who collected the ice core; the National Ice Core  
Facility for ice core storage and processing; Michael Kalk for his help on lab work with the samples, and the many  
student researchers who produced data from the SPC14 ice core.

520

525

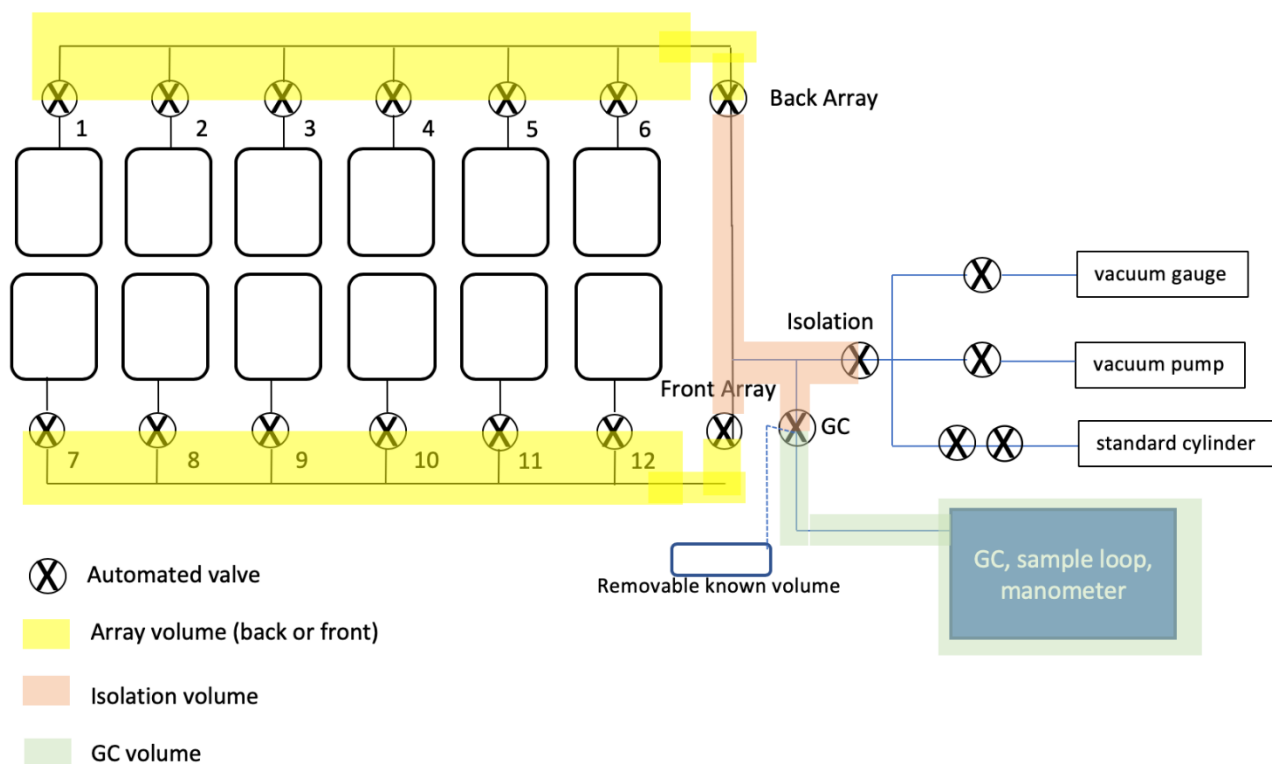
530



535

**Figure 1: Total air content of the SPC14 ice core.** (Left) Individual measurements are shown, plotted on the SP19 ice age scale (Winski et al., 2019). Black line is the smoothed record using a running 10-point average. TAC is expressed in units of  $\text{cm}^3$  air at standard temperature and pressure, per gram of ice. Orange markers are TAC measurements collected at OSU (depths 130 – 841m, 1150-1751 m, pooled standard deviation =  $0.0006 \text{ cm}^3\text{g}^{-1}$ ).

540 Blue markers are TAC measurements collected at PSU (depths 130-1150 m, pooled standard deviation =  $0.002 \text{ cm}^3\text{g}^{-1}$ ). (Right) Ice age as a function of depth. Data from Winski et al. (2019).



545

**Figure 2: Schematic of extraction line and GC for TAC and CH<sub>4</sub> measurements.** Diagram includes a removable known volume, which was used in the  $T_{eff}$  calibration (see text). Numbered valves are individual flask valves. Air released during the melt phase is trapped between the flask and the numbered automated valve. Yellow: Back and front array volumes. Light orange: isolation volume, includes the vacuum line between the array valves, the isolation valve, and the GC valve. Green: GC volume, includes the vacuum line between the GC valve and the GC sample loop. All volumes are listed in Table 1.

550

555

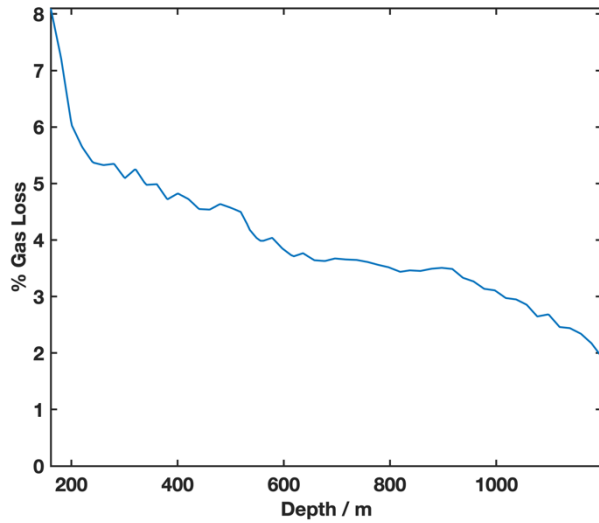
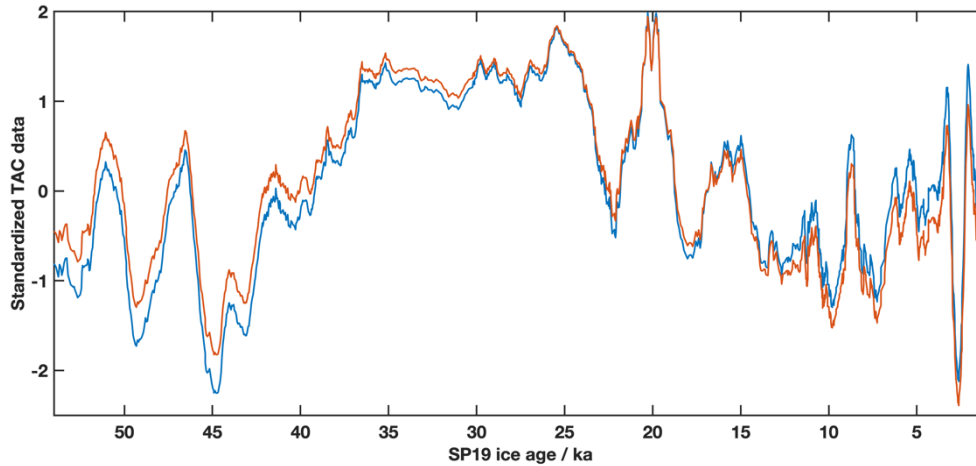


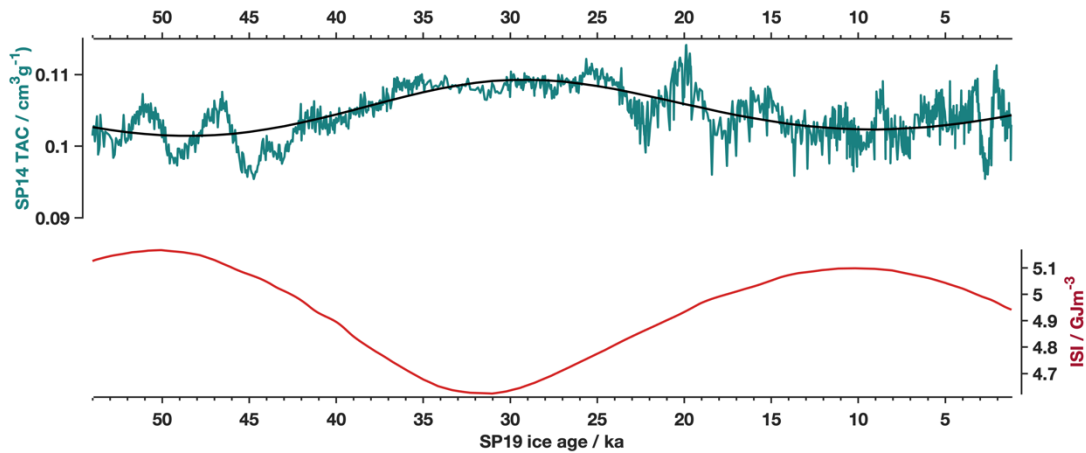
**Figure 3: Cut bubble correction for SPC14 ice core.** Gas loss due to cut bubbles plotted with depth. Cut bubble corrections range from 8 % decreasing to 1.9 % gas loss at the base of the bubbly ice.

575

580

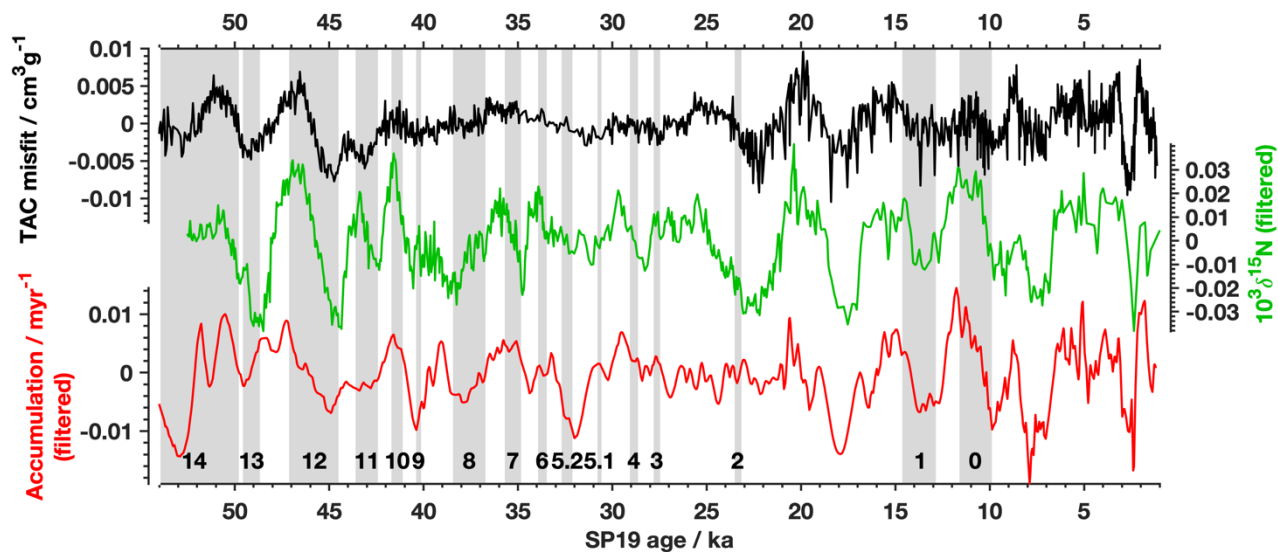


585 **Figure 4. Comparison of TAC and the non-thermal residual.** The non-thermal residual quantity, explained in section 3.2, explains how much temperature affects TAC through the ideal gas law. The TAC and non-thermal residual are nearly identical, indicating a very small direct effect of temperature on TAC. Blue: A standardized version of the SPC14 TAC record. Orange: Following Raynaud et al. (2007), the standardized TAC data after correcting for the direct effects of temperature ( $V_{cr}$ ) (Martiniere et al., 1992). Both records were smoothed using a 10-point moving average, to better highlight the difference.



590

**Figure 5: SPC14 TAC predicted from integrated solar insolation (ISI)** Top: SPC14 TAC (green) and predicted by linear regression of TAC with ISI using a cutoff threshold of  $225 \text{ Wm}^{-2}$  (black).  $R^2 = 0.46$ ,  $p < 0.0001$ ,  $b = 0.194$ ,  $m = -0.0173$ . Bottom: ISI at  $90^\circ\text{S}$  using a cutoff threshold of  $225 \text{ Wm}^{-2}$ .



595 **Figure 6: TAC, accumulation rate, and  $\delta^{15}N-N_2$ .** TAC misfit (black, upper) compared with  $\delta^{15}N-N_2$  (green, middle: Winski et al. (2019) accumulation rate (red, bottom: Kahle et al., 2021). Both the  $\delta^{15}N-N_2$  data and accumulation rate were filtered using a highpass filter removing variability with period greater than 10,000 years prior to comparison. TAC misfit was plotted on the SP19 ice age scale. The highpass filtered  $\delta^{15}N-N_2$  is plotted on the SP19 gas age scale (Middle: Epifanio et al., 2019). The highpass filtered accumulation rate on the SP19 ice age scale (Bottom: Winski et al., 2019). Grey shaded areas are D-O 600 events, numbered on the bottom for reference. Correlation coefficients are presented in Table 2.

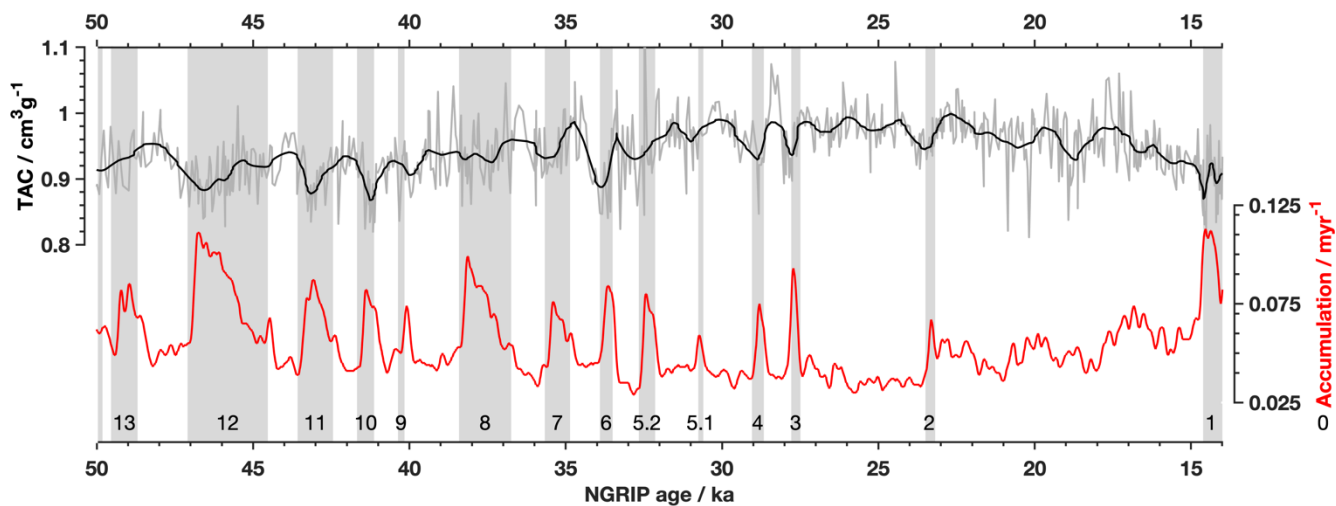
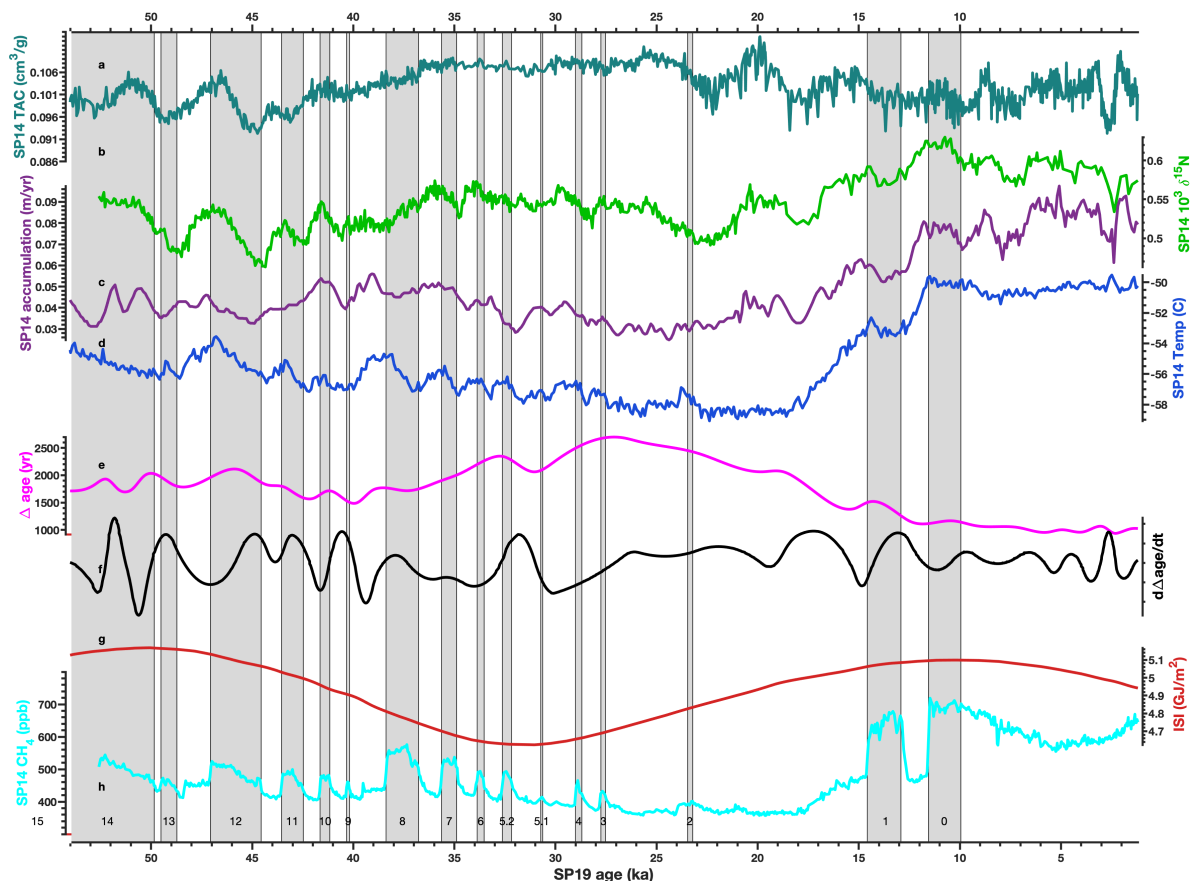


**Figure 7: Greenland (NGRIP) TAC and accumulation rate.** TAC (grey, upper: Eicher et al., 2016) compared  
 605 with accumulation rate (red, bottom: Kindler et al., 2014). Black line is smoothed TAC using a 10-point running  
 average. Grey shaded areas are D-O events, numbered on the bottom for reference. Correlation coefficients are  
 presented in Table 4.

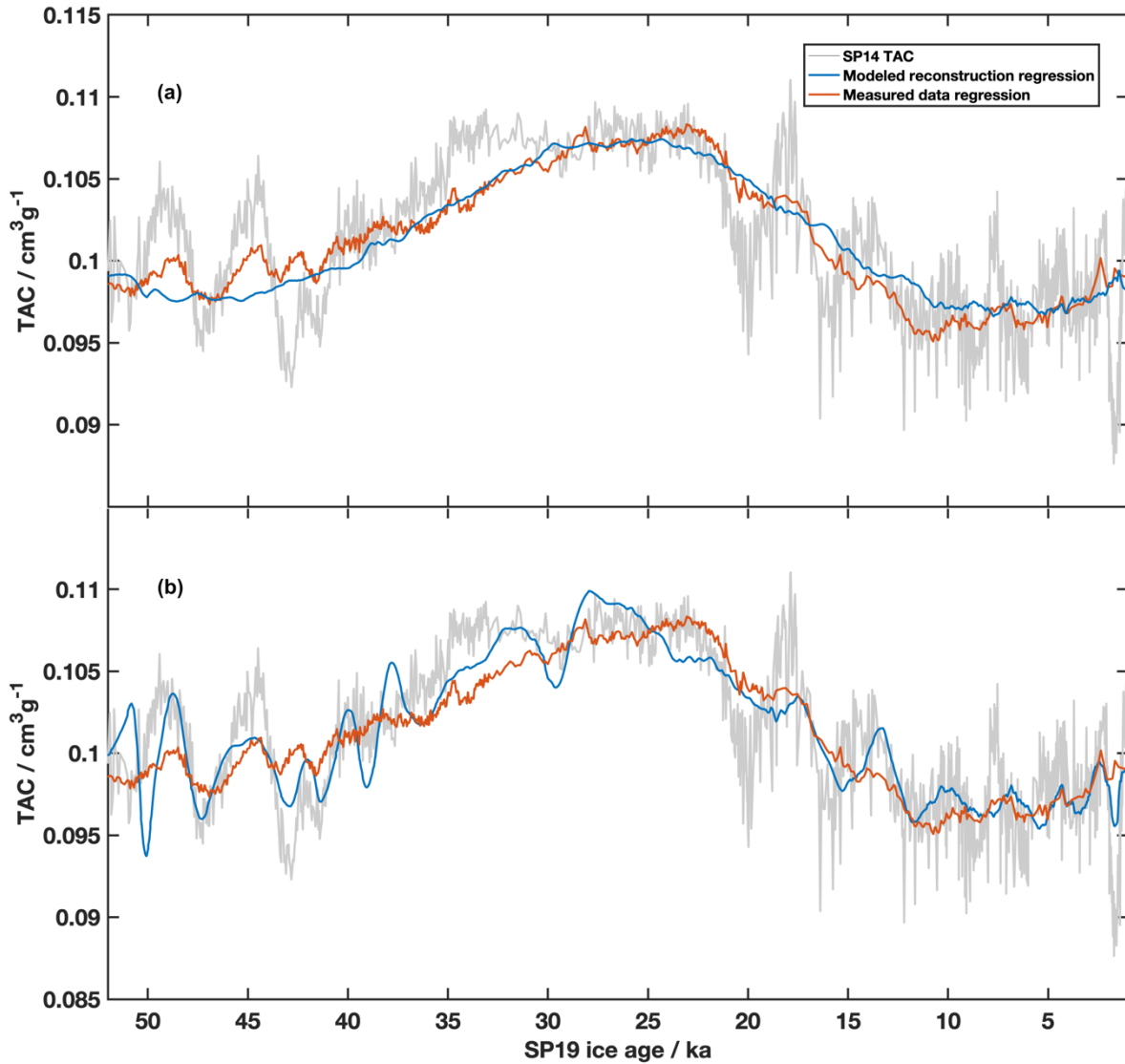
610





615

**Figure 8: TAC record of SPC14 ice core and other climate proxies.** a) SPC14 TAC record. Mean value of duplicate measurements, plotted on the ice age scale. b)  $\delta^{15}N-N_2$ , plotted on the gas age scale (Winski et al., 2019). c) Accumulation rate plotted on the ice age scale. For the last 11.3 ka the accumulation rate was constrained by layer counting of seasonal variations of magnesium and calcium ions (Winski et al., 2019). For older time periods, accumulation is modeled using an  
 620 inverse method (Winski et al., 2019, Kahle et al., 2021). D)  $\delta^{18}O_{ice}$  a local temperature proxy (Kahle et al., 2021). e) SPC14  $\Delta$ age, empirically derived using independent gas and ice age markers (Epifanio et al., 2020) f) Derivative of  $\Delta$ age. g) Integrated Summer Insolation (ISI), at a cutoff threshold of  $225 \text{ Wm}^{-2}$ , at  $90^\circ \text{ S}$  (Huybers et al., 2006). h) SPC14  $\text{CH}_4$ , plotted on the gas age scale, added for chronological orientation (Epifanio et al., 2020). Grey bars are numbered and represent D-O events for reference.



625

**Figure 9: Multiple regressions of TAC compared to SPC14 TAC record.** a) SPC14 TAC data (grey), modeled reconstruction multiple regression using ISI and modeled reconstructions of accumulation rate ( $r^2 = 0.51$ ,  $p < 0.001$ ) (blue), measured data multiple regression which includes  $\delta^{15}N-N_2$  and ISI ( $r^2 = 0.62$ ,  $p < 0.001$ ) (orange). b) Multiple regression comparison including  $\delta\Delta\text{age}/\delta t$ . SPC14 TAC data (grey), multiple regression using modeled reconstructions of temperature

630 and accumulation rate, including  $\delta\Delta\text{age}/\delta t$  ( $r^2 = 0.76$ ,  $p < 0.001$ ) (blue), multiple regression using measured parameters including  $\delta\Delta\text{age}/\delta t$  ( $r^2 = 0.77$ ,  $p < 0.001$ ) (orange).

**Table 1: Volumes of CH<sub>4</sub> extraction line.** Volumes of CH<sub>4</sub> extraction line. Volumes listed correspond to highlighted areas in Fig. 2.

635

<b>Line</b>	<b>Volume (cc)</b>
Removable Known Volume	22.14
Front Array	28.45
Total	65.03
GC to isolation space	16.90
Isolation Space	6.19

**Table 2: Pearson correlation coefficients of single regressions.** Pearson correlation coefficients of single regressions.

640 Highpass-filtered records were filtered using a bandpass filter that eliminated frequencies greater than 10,000 years.

	<b>TAC</b>	<b>Highpass filtered TAC</b>
$\delta^{15}N-N_2$	0.13	0.25
$\delta^{15}N-N_2$ (highpass)	0.25	0.51
Accumulation	-0.20	0.18
Accumulation (highpass)	0.18	0.59
$\delta^{18}O_{ice}$	-0.39	0.10
$\delta^{18}O_{ice}$ (highpass)	0.11	-0.13
Temperature	-0.37	0.11
Temperature (highpass)	0.11	0.05

645

650 **Table 3: Multiple regressions of TAC with other ice core variables.** Parameter listed is the term considered in the regression. Parameters are listed in the order of how much adjusted  $r^2$  changes when the parameter is removed from to the regression. All factors listed are statistically significant (null hypothesis,  $p < 0.05$ ). Left: terms of multiple regression when using modeled reconstructions for ISI and accumulation rate ( $r^2 = 0.51$ ). Right: terms of multiple regression of TAC when using measured parameters ( $r^2 = 0.62$ ).

655

Modeled reconstruction multiple regression		Measured parameter multiple regression	
Parameter	% Change in adjusted $r^2$	Parameter	% Change in adjusted $r^2$
ISI	27	ISI	40
Accumulation	3	$\delta^{15}N-N_2$	13

## References

Arnaud, L., Modélisation de la Transformation de la Neige en Glace à la Surface des Calottes Polaires; étude du Transport des gaz dans ces Milieux Poreux, PhD. Université Joseph Fourier, tel-00709566, version 1 (19-06-2012), 1997.

660

Arnaud, L., Barnola, J. M., and Duval, P.: Physical modeling of the densification of snow/firn and ice in the upper part of polar ice sheets, in: Physics of Ice Core Records, pp. 285-305. Hokkaido University Press, <http://hdl.handle.net/2115/32472>, 2000.

665 Bazin, L., Landais, A., Lemieux-Dudon, B., Toyé Mahamadou Kele, H., Veres, D., Parrenin, F., Martinerie, P., Ritz, C., Capron, E., Lipenkov, V., Loutre, M.-F., Raynaud, D., Vinther, B., Svensson, A., Rasmussen, S. O., Severi, M., Blunier, T., Leuenberger, M., Fischer, H., Masson-Delmotte, V., Chappellaz, J., and Wolff, E.: An optimized multi-proxy, multi-site Antarctic ice and gas orbital chronology (AICC2012): 120–800 ka, *Clim. Past*, 9, 1715–1731, <https://doi.org/10.5194/cp-9-1715-2013>, 2013.

670

Buizert, C., Fudge, T. J., Roberts, W. H. G., Steig, E. J., Sherriff-Tadano, S., Ritz, C., Lefebvre, E., Edwards, J., Kawamura, K., Oyabu, I., Motoyama, H., Kahle, E. C., Jones, T. R., Abe-Ouchi, A., Obase, T., Martin, C., Corr, H., Severinghaus, J. P., Beaudette, R., Epifanio, J. A., Brook, E. J., Martin, K., Chappellaz, J., Aoki, S., Nakazawa,

T., Sowers, T. A., Alley, R. B., Ahn, J., Sigl, M., Severi, M., Dunbar, N. W., Svensson, A., Fegyveresi, J. M., He,  
675 C., Liu, Z., Zhu, J., Otto-Bliesner, B. L., Lipenkov, V. Y., Kageyama, M., and Schwander, J.: Antarctic surface  
temperature and elevation during the Last Glacial Maximum, *Science*, 372, 1097–1101,  
<https://doi.org/10.1126/science.abd2897>, 2021.

Courville, Z. R., Albert, M. R., Fahnestock, M. A., Cathles IV, L. M., and Shuman, C. A.: Impacts of an  
680 accumulation hiatus on the physical properties of firn at a low-accumulation polar site, *J. Geophys. Res. Earth  
Surf.*, 112, <https://doi.org/10.1029/2005JF000429>, 2007.

Eicher, O., Baumgartner, M., Schilt, A., Schmitt, J., Schwander, J., Stocker, T. F., and Fischer, H.: Climatic and  
insolation control on the high-resolution total air content in the NGRIP ice core, *Clim. Past*, 12, 1979, 2016.

685

Epifanio, J. A., South Pole ice core (SPC14) total air content (TAC), U.S. Antarctic Program (USAP) Data Center.  
doi: <https://doi.org/10.15784/601546>, 2022.

Epifanio, J. A., Brook, E. J., Buizert, C., Edwards, J. S., Sowers, T. A., Kahle, E. C., Severinghaus, J. P., Steig,  
690 E. J., Winski, D. A., Osterberg, E. C., Fudge, T. J., Aydin, M., Hood, E., Kalk, M., Kreutz, K. J., Ferris, D. G.,  
and Kennedy, J. A.: The SP19 chronology for the South Pole Ice Core – Part 2: gas chronology,  $\Delta$ age, and  
smoothing of atmospheric records, *Clim. Past*, 16, 2431–2444, <https://doi.org/10.5194/cp-16-2431-2020>, 2020.

Fegyveresi, J. M., Alley, R. B., Spencer, M. K., Fitzpatrick, J. J., Steig, E. J., White, J. W. C., McConnell, J. R.,  
695 and Taylor, K. C.: Late-Holocene climate evolution at the WAIS Divide site, West Antarctica: bubble number-  
density estimates, *J. Glaciol.*, 57, 629–638, <https://doi.org/10.3189/002214311797409677>, 2011.

Fegyveresi, John M. Physical properties of the West Antarctic Ice Sheet (WAIS) Divide deep core: Development,  
evolution, and interpretation. The Pennsylvania State University, UMI: 37155012015.

700

Fegyveresi, J.M., Alley, R.B., Fitzpatrick, J.J., Voigt, D., Courville, Z. and Lieblappen, R., 2018, December.  
Measurement and interpretation of bubble number-density evolution through the upper 1200 meters of the  
SPC14 South Pole Ice Core (SPICEcore). In: AGU Fall Meeting Abstracts, December 2018, Washington D.C.,  
C41C-1750, 2018AGUFM.C41C1750F, 2018.

705

Fitzpatrick, J. J., Voigt, D. E., Fegyveresi, J. M., Stevens, N. T., Spencer, M. K., Cole-Dai, J., Alley, R. B., Jardine, G. E., Cravens, E. D., Wilen, L. A., Fudge, T. J., and McConnell, J. R.: Physical properties of the WAIS Divide ice core, *J. Glaciol.*, 60, 1181–1198, <https://doi.org/10.3189/2014JoG14J100>, 2014.

710 Fudge, T. J., Lilien, D. A., Koutnik, M., Conway, H., Stevens, C. M., Waddington, E. D., Steig, E. J., Schauer, A. J., and Holschuh, N.: Advection and non-climate impacts on the South Pole Ice Core, *Clim. Past*, 16, 819–832, <https://doi.org/10.5194/cp-16-819-2020>, 2020.

Golledge, N. R., Levy, R. H., McKay, R. M., Fogwill, C. J., White, D. A., Graham, A. G. C., Smith, J. A.,  
715 Hillenbrand, C.-D., Licht, K. J., Denton, G. H., Ackert, R. P., Maas, S. M., and Hall, B. L.: Glaciology and geological signature of the Last Glacial Maximum Antarctic ice sheet, *Quat. Sci. Rev.*, 78, 225–247, <https://doi.org/10.1016/j.quascirev.2013.08.011>, 2013.

Goodwin, I. D., Browning, S., Lorrey, A. M., Mayewski, P. A., Phipps, S. J., Bertler, N. A. N., Edwards, R. P.,  
720 Cohen, T. J., van Ommen, T., Curran, M., Barr, C., and Stager, J. C.: A reconstruction of extratropical Indo-Pacific sea-level pressure patterns during the Medieval Climate Anomaly, *Clim. Dyn.*, 43, 1197–1219, <https://doi.org/10.1007/s00382-013-1899-1>, 2014.

Gregorich, M., Strohmaier, S., Dunkler, D., and Heinze, G.: Regression with Highly Correlated Predictors:  
725 Variable Omission Is Not the Solution, *Int. J. Environ. Res. Public Health*, 18, 4259, <https://doi.org/10.3390/ijerph18084259>, 2021.

Gregory, S. A., Albert, M. R., and Baker, I.: Impact of physical properties and accumulation rate on pore close-off in layered firn, *The Cryosphere*, 8, 91–105, 2014.

730

Huybers, P.: Early Pleistocene glacial cycles and the integrated summer insolation forcing, *Science*, 313, 508–511, 2006.

Kahle, E. C., Steig, E. J., Jones, T. R., Fudge, T., Koutnik, M. R., Morris, V. A., Vaughn, B. H., Schauer, A. J.,  
735 Stevens, C. M., Conway, H., and others: Reconstruction of temperature, accumulation rate, and layer thinning

from an ice core at South Pole, using a statistical inverse method, *J. Geophys. Res. Atmospheres*, 126, e2020JD033300, 2021.

740 Krinner, G., Raynaud, D., Doutriaux, C., and Dang, H.: Simulations of the Last Glacial Maximum ice sheet surface  
climate: Implications for the interpretation of ice core air content, *J. Geophys. Res.-Atmospheres*, 105, 2059–  
2070, <https://doi.org/10.1029/1999jd900399>, 2000.

745 Lee, J. E., Brook, E. J., Bertler, N. A. N., Buizert, C., Baisden, T., Blunier, T., Ciobanu, V. G., Conway, H., Dahl-  
Jensen, D., Fudge, T. J., Hindmarsh, R., Keller, E. D., Parrenin, F., Severinghaus, J. P., Vallelonga, P.,  
Waddington, E. D., and Winstrup, M.: An 83\,000-year-old ice core from Roosevelt Island, Ross Sea, Antarctica,  
*Clim. Past*, 16, 1691–1713, <https://doi.org/10.5194/cp-16-1691-2020>, 2020.

750 Lilien, D. A., Fudge, T. J., Koutnik, M. R., Conway, H., Osterberg, E. C., Ferris, D. G., Waddington, E. D., and  
Stevens, C. M.: Holocene Ice-Flow Speedup in the Vicinity of the South Pole, *Geophys. Res. Lett.*, 45, 6557–  
6565, <https://doi.org/10.1029/2018GL078253>, 2018.

755 Lipenkov, V. Y., Raynaud, D., Loutre, M. F., and Duval, P.: On the potential of coupling air content and O-2/N-  
2 from trapped air for establishing an ice core chronology tuned on local insolation, *Quat. Sci. Rev.*, 30, 3280–  
3289, <https://doi.org/10.1016/j.quascirev.2011.07.013>, 2011.

Martinerie, P., Raynaud, D., Etheridge, D. M., Barnola, J.-M., and Mazaudier, D.: Physical and climatic  
parameters which influence the air content in polar ice, *Earth Planet. Sci. Lett.*, 112, 1–13, 1992.

760 Martinerie, P., Lipenkov, V. Y., Raynaud, D., Chappellaz, J., Barkov, N. I., and Lorius, C.: Air content paleo  
record in the Vostok ice core (Antarctica): A mixed record of climatic and glaciological parameters, *J. Geophys.  
Res. Atmospheres*, 99, 10565–10576, 1994.

Martinerie, P., Lipenkov, V. Y., and Raynaud, D.: Correction of Air-Content Measurements in Polar Ice for the  
Effect of Cut Bubbles at the Surface of the Sample, *J. Glaciol.*, 5, n.d.

765 Mischler, J. A., Sowers, T. A., Alley, R. B., Battle, M., McConnell, J. R., Mitchell, L., Popp, T., Sofen, E., and  
Spencer, M. K.: Carbon and hydrogen isotopic composition of methane over the last 1000 years, *Glob.*  
*Biogeochem. Cycles*, 23, <https://doi.org/10.1029/2009GB003460>, 2009.

Mitchell, L. E., Brook, E. J., Sowers, T., McConnell, J. R., and Taylor, K.: Multidecadal variability of atmospheric  
770 methane, 1000–1800 CE, *J. Geophys. Res. Biogeosciences*, 116, 2011.

Mitchell, L. E., Buizert, C., Brook, E. J., Breton, D. J., Fegyveresi, J., Baggenstos, D., Orsi, A., Severinghaus, J.,  
Alley, R. B., Albert, M., Rhodes, R. H., McConnell, J. R., Sigl, M., Maselli, O., Gregory, S., and Ahn, J.:  
Observing and modeling the influence of layering on bubble trapping in polar firn, *J. Geophys. Res. Atmospheres*,  
775 120, 2558–2574, <https://doi.org/10.1002/2014jd022766>, 2015.

Morgan, J. D., Buizert, C., Fudge, T. J., Kawamura, K., Severinghaus, J. P., and Trudinger, C. M.: Gas isotope  
thermometry in the South Pole and Dome Fuji ice cores provides evidence for seasonal rectification of ice core  
gas records, *The Cryosphere*, 16, 2947–2966, <https://doi.org/10.5194/tc-16-2947-2022>, 2022.

780

NOAA, US Department of Commerce, Global Monitoring Laboratory - Data Visualization. url:  
<https://gml.noaa.gov/dv/>, (date accessed: Nov 19, 2021.)

Parrenin, F., Jouzel, J., Kawamura, K., Lemieux-Dudon, B., Loulergue, L., Masson-Delmotte, V., Narcisi, B.,  
785 Raisbeck, G., Raynaud, D., Ruth, U., Schwander, J., Severi, M., Spahni, R., Steffensen, J. P., Svensson, A., Udisti,  
R., Waelbroeck, C., and Wolff, E.: The EDC3 chronology for the EPICA Dome C ice core, *Clim Past*, 13, 2007.

Raphael, M. N., Marshall, G. J., Turner, J., Fogt, R. L., Schneider, D., Dixon, D. A., Hosking, J. S., Jones, J. M.,  
and Hobbs, W. R.: The Amundsen Sea Low: Variability, Change, and Impact on Antarctic Climate, *Bull. Am.*  
790 *Meteorol. Soc.*, 97, 111–121, <https://doi.org/10.1175/BAMS-D-14-00018.1>, 2016.

Raynaud, D. and Lebel, B.: Total gas content and surface elevation of polar ice sheets, *Nature*, 281, 289,  
<https://doi.org/10.1038/281289a0>, 1979.



- 795 Raynaud, D. and Lorius, C.: Climatic Implications of Total Gas Content in Ice at Camp Century, *Nature*, 243, 283, <https://doi.org/10.1038/243283a0>, 1973.
- Raynaud, D., Chappellaz, J., Ritz, C., and Martinerie, P.: Air content along the Greenland Ice Core Project core: A record of surface climatic parameters and elevation in central Greenland, *J. Geophys. Res. Oceans*, 102, 26607–26613, 1997.
- 800
- Raynaud, D., Lipenkov, V., Lemieux-Dudon, B., Duval, P., Loutre, M.-F., and Lhomme, N.: The local insolation signature of air content in Antarctic ice. A new step toward an absolute dating of ice records, *Earth Planet. Sci. Lett.*, 261, 337–349, <https://doi.org/10.1016/j.epsl.2007.06.025>, 2007.
- 805 Saltykov, S. A.: *Stereometričeskaâ metallografiâ:(stereologiâ metalličeskikh materialov)*, Metallurgiiâ, 1976.
- Schneider, D. P., Okumura, Y., and Deser, C.: Observed Antarctic Interannual Climate Variability and Tropical Linkages, *J. Clim.*, 25, 4048–4066, <https://doi.org/10.1175/JCLI-D-11-00273.1>, 2012.
- Schwander, J.: The transformation of snow to ice and the occlusion of gases, *Environ. Rec. Glaciers Ice Sheets*,  
810 53–67, 1989.
- Severinghaus, J. P., Sowers, T., Brook, E. J., Alley, R. B., and Bender, M. L.: Timing of abrupt climate change at the end of the Younger Dryas interval from thermally fractionated gases in polar ice, *Nature*, 391, 141–146, 1998.
- 815 Sowers, T., Bender, M., Raynaud, D., and Korotkevich, Y. S.:  $\delta^{15}\text{N}$  of  $\text{N}_2$  in air trapped in polar ice: A tracer of gas transport in the firn and a possible constraint on ice age-gas age differences, *J. Geophys. Res. Atmospheres*, 97, 15683–15697, <https://doi.org/10.1029/92JD01297>, 1992.
- WAIS Divide Project Members, Fudge, T. J., Steig, E. J., Markle, B. R., Schoenemann, S. W., Ding, Q., Taylor,  
820 K. C., McConnell, J. R., Brook, E. J., Sowers, T., White, J. W. C., Alley, R. B., Cheng, H., Clow, G. D., Cole-Dai, J., Conway, H., Cuffey, K. M., Edwards, J. S., Lawrence Edwards, R., Edwards, R., Fegyveresi, J. M., Ferris, D., Fitzpatrick, J. J., Johnson, J., Hargreaves, G., Lee, J. E., Maselli, O. J., Mason, W., McGwire, K. C., Mitchell, L. E., Mortensen, N., Neff, P., Orsi, A. J., Popp, T. J., Schauer, A. J., Severinghaus, J. P., Sigl, M., Spencer, M. K., Vaughn, B. H., Voigt, D. E., Waddington, E. D., Wang, X., and Wong, G. J.: Onset of deglacial warming in  
825 West Antarctica driven by local orbital forcing, *Nature*, 500, 440–444, <https://doi.org/10.1038/nature12376>, 2013.

Winski, D. A., Fudge, T. J., Ferris, D. G., Osterberg, E. C., Fegyveresi, J. M., Cole-Dai, J., Thundercloud, Z., Cox, T. S., Kreutz, K. J., Ortman, N., Buizert, C., Epifanio, J., Brook, E. J., Beaudette, R., Severinghaus, J., Sowers, T., Steig, E. J., Kahle, E. C., Jones, T. R., Morris, V., Aydin, M., Nicewonger, M. R., Casey, K. A., Alley, 830 R. B., Waddington, E. D., Iverson, N. A., Dunbar, N. W., Bay, R. C., Souney, J. M., Sigl, M., and McConnell, J. R.: The SP19 chronology for the South Pole Ice Core – Part 1: volcanic matching and annual layer counting, *Clim. Past*, 15, 1793–1808, <https://doi.org/10.5194/cp-15-1793-2019>, 2019.